Low-Complexity Dual-Vector-Based Predictive Control of Three-Phase PWM Rectifiers Without Duty-Cycle Optimization

XIAOLONG SHI [1], (Student Member, IEEE), **JIANGUO ZHU** [2], (Senior Member, IEEE),
LI LI [1], (Member, IEEE), AND **DYLAN DAH-CHUAN LU** [1], (Senior Member, IEEE)
[1]School of Electrical and Data Engineering, University of Technology Sydney, Sydney, NSW 2007, Australia
[2]School of Electrical and Information Engineering, The University of Sydney, Sydney, NSW 2006, Australia

Corresponding author: Xiaolong Shi (sydney3168@gmail.com)

ABSTRACT The conventional model-predictive-based direct power control (MPDPC) of the three-phase full-bridge AC/DC converters chooses the best single voltage vector for the following control period, which results in variable switching frequency and power distortion, and thus a relatively higher sampling frequency is needed to achieve acceptable results. This paper proposes a simplified dual-vector-based predictive direct duty-cycle-control (SPDDC) with an additional zero vector implemented in contrast to the MPDPC. With the same best vector selection method, the proposed strategy has retained the control simplicity with just one more step added and much better control performance as well as a fixed switching frequency in comparison to the MPDPC. On the other hand, the duty-cycle optimization procedure is eliminated while the negative duration issue is essentially resolved compared with the conventional dual-vector-based model predictive duty-cycle-control (MPDCC). Comprehensive comparisons of various control methods by numerical simulation and experimental testing show that the SPDDC can achieve better steady state and dynamic performance than the MPDPC and simpler algorithms than the MPDCC.

I. INTRODUCTION

The three-phase full-bridge AC/DC converter is a popular device widely applied in various applications, such as integration of renewable energy resources, electric drives, voltage source converter transmission, and so on. It has several merits such as four-quadrants power control, flexible DC voltage control, and low DC capacitance with high-quality DC voltage [1]–[4].

The classical voltage-oriented control (VOC) method controls the input power by regulating the decoupled AC currents [5]. Although it has good dynamic and steady state performance, the main drawback is that VOC highly depends on the inner current controller and coordinate transformation accuracy. Similar to the direct torque control (DTC) of electrical machine drive, the conventional switching-table-based direct power control (STDPC) regulates the power directly by choosing one voltage vector from a predefined switching

table [6]–[9]. However, the STDPC bears with variable switching frequency and irregular power ripples because of the use of hysteresis comparators and switching tables, resulting in broadband harmonic spectrum range, which requires high sampling frequency for the acceptable performance.

To improve the performance of STDPC, various kinds of methods have been combined with the direct power control (DPC), such as the fuzzy logic, space vector modulation (SVM), sliding mode, virtual flux, and model predictive control [10]–[15]. The model-predictive-based direct power control (MPDPC) is a quite popular control method in the area of power converters and motor drives along with control unit development, since it is a promising algorithm with advantages like rapid instantaneous response, no need of modulator, and flexibility to add various constraints [13], [16]–[22]. Though the power ripples can be reduced compared with the STDPC, the MPDPC still cannot achieve satisfactory steady state performance since only one single switching vector selected in each control period and limited number of voltage vectors. Besides, its switching frequency is not

The associate editor coordinating the review of this manuscript and approving it for publication was Dušan Grujić [.]

constant, leading to the spread spectrum nature of harmonics and complicated filter design.

Various control methods have been proposed in the literature to further enhance the control performance and realize the fixed switching frequency by implementing two or more vectors in one control section. In [23]–[31], the concept of duty-cycle-control and SVM-based methods have been introduced and studied. The SVM-based method obtains the desired vector by nullifying the error of the control variable at the end of the following control period, which uses the SVM to generate the gating pulses [12], [27]. The three-vector-based duty-cycle-control in [23] and [24] obtains the best adjacent non-zero vector pair and a zero vector by sector information, namely the grid-voltage vector location. However, the sector information-based vector selection algorithm might select the non-best vectors [25], this further results in negative duration value and power control deterioration, such as significant power notches and current spikes. To solve this issue, in [25] and [26], a complementary vector sequence table is added with an additional vector sequence table, but the negative duration issue cannot be fully solved after recalculation. The authors in [27] proposed an improved method without selecting the voltage vectors, but it needs a procedure of equivalent reconstruction of switching signals. Therefore, for multi-vector-based duty-cycle-control, using sector information for the best non-zero vector selection is not a good choice since the negative duration issue could be serious. Recently, the popular and effective solution is to use the model predictive control method for the best vector selection, it has been applied in several multi-vector-based approaches [28]–[33], while the procedure of determining these vectors become more complex [10], [33]. Taking advantage of the feature that the power variation rates of reversible vector pair are symmetrical for that of zero vector, the proposed three-vector-based method with reversible vector selection in [33] cunningly resolved the negative duration issue. However, the control complexity is also increased in comparison to the MPDPC and dual-vector-based methods.

Apart from the efforts on the improvement of best vector or vector pair selection, the significantly increased computational burden on hardware from the vector duration calculation should also be considered, since the least-square optimization method is generally employed in the above two or three-vector-based duty-cycle-control methods [25]–[31], [33]. The duration calculation approach is computationally intensive since the active and reactive power slope calculations of the selected vectors are needed [30]. Meanwhile, the negative duration of zero vector cannot be avoided especially during the dynamic instant with large instantaneous power errors, and thus the compensation measure of negative duration issue is also needed, which further increases the control complexity. By emulating the SVM strategy, the modulated model predictive control (MMPC) in [32] uses a different method to derive the durations simply. However, it employs two complicated cost

functions for the best vector pair selection and only selects the adjacent non-zero vector pair with or without the zero vector. The performance is not evaluated compared with other multi-vector-based methods. Some new insights on reducing the calculation burden of vector selection and duration have been provided in [34]–[36]. The algorithms for vector selection and duration calculation are reconstructed from the SVM-based method in [34] and from different control objectives in [35], [36], which are still quite complex and not intuitive.

To overcome the critical issues such as complicated vector selection approach and high computational burden of durations, this paper proposes a simplified predictive direct duty-cycle (SPDDC) approach. The SPDDC can solve the negative duration issue essentially and simplify the control scheme by eliminating the duty-cycle optimization. Firstly, the cost function of MPDPC is employed to choose the best active voltage vector to avoid selecting the non-optimal vectors. Then, the duty-cycle is derived directly by using the cost function value obtained by applying the selected vectors without compensation and optimization. It can thus eliminate the calculation of power slopes and reduce the computational burden. While the negative duration is essentially avoided, the merits, such as good steady state and dynamic performance, of the duty-cycle-control are retained. The control algorithm is more intuitive with better performance compared with the conventional methods. Numerical simulation and experiments have been conducted and the results discussed to confirm the theoretical analyses and the advantages of the novel method.

II. MODELING OF THREE-PHASE GRID-CONNECTED CONVERTER

Fig.1 shows a topology of the three-phase full-bridge grid-connected AC/DC converter, which is connected to the main AC power supply via three inductors, L, and resistors, R, where e_a, e_b, and e_c are the electromotive forces (*emf*) of three-phase AC power source; v_a, v_b, and v_c the three-phase terminal voltages; and i_a, i_b, and i_c the three-phase currents. At the DC side, a DC load is connected to the DC bus in parallel to a capacitor C.
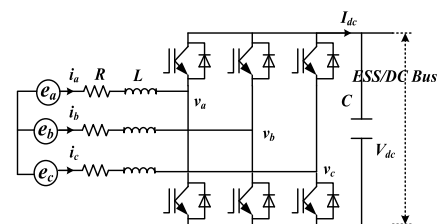

FIGURE 1. Topology of the AfC/DC three-phase converter.

In the $\alpha\beta$-coordinate system, the AC power source *emf* and current vectors, $e_{\alpha\beta}$ and $i_{\alpha\beta}$, can be derived from the

three-phase *emf* and currents, respectively, as

$$e_{\alpha\beta} = \begin{bmatrix} e_\alpha \\ e_\beta \end{bmatrix} = \frac{2}{3} \begin{bmatrix} 1 & -1/2 & -1/2 \\ 0 & \sqrt{3}/2 & -\sqrt{3}/2 \end{bmatrix} \begin{bmatrix} e_a \\ e_b \\ e_c \end{bmatrix} \quad (1)$$

$$i_{\alpha\beta} = \begin{bmatrix} i_\alpha \\ i_\beta \end{bmatrix} = \frac{2}{3} \begin{bmatrix} 1 & -1/2 & -1/2 \\ 0 & \sqrt{3}/2 & -\sqrt{3}/2 \end{bmatrix} \begin{bmatrix} i_a \\ i_b \\ i_c \end{bmatrix} \quad (2)$$

The line currents can be calculated by solving

$$e_{\alpha\beta} = L\frac{di_{\alpha\beta}}{dt} + Ri_{\alpha\beta} + v_{\alpha\beta} \quad (3)$$

where $v_{\alpha\beta}$ is the terminal voltage vector in the $\alpha\beta$-coordinate system. The exchange between the active power P and the reactive power Q can be derived as

$$\begin{bmatrix} P \\ Q \end{bmatrix} = \frac{3}{2} \begin{bmatrix} e_\alpha & e_\beta \\ e_\beta & -e_\alpha \end{bmatrix} \begin{bmatrix} i_\alpha \\ i_\beta \end{bmatrix} \quad (4)$$

III. MODEL-PREDICTIVE-BASED DUTY-CYCLE- CONTROL

A typical dual-vector-based model predictive duty-cycle-control (MPDCC) method is presented in [30]. The power differential equation can be derived from (4) as

$$\frac{d}{dt}\begin{bmatrix} P \\ Q \end{bmatrix} = \frac{3}{2}\left(i_\alpha \frac{d}{dt}\begin{bmatrix} e_\alpha \\ e_\beta \end{bmatrix} + \frac{di_\alpha}{dt}\begin{bmatrix} e_\alpha \\ e_\beta \end{bmatrix} \right.$$
$$\left. + i_\beta \frac{d}{dt}\begin{bmatrix} e_\beta \\ -e_\alpha \end{bmatrix} + \frac{di_\beta}{dt}\begin{bmatrix} e_\beta \\ -e_\alpha \end{bmatrix} \right) \quad (5)$$

In the complex form, the sinusoidal and balanced three-phase *emf* can be expressed in the $\alpha\beta$-coordinate system as

$$e = e_\alpha + je_\beta = |e|e^{j\omega t} \quad (6)$$

where ω is the grid angular frequency. Taking derivatives on the both sides of (6) yields

$$\frac{d}{dt}\begin{bmatrix} e_\alpha \\ e_\beta \end{bmatrix} = \omega \cdot \begin{bmatrix} -e_\beta \\ e_\alpha \end{bmatrix} \quad (7)$$

Substituting (3), (4) and (7) into (5), one obtains

$$\frac{d}{dt}\begin{bmatrix} P_i \\ Q_i \end{bmatrix} = -\frac{R}{L}\begin{bmatrix} P_i \\ Q_i \end{bmatrix} + \omega \begin{bmatrix} -Q_i \\ P_i \end{bmatrix}$$
$$+ \frac{3}{2L}\begin{bmatrix} (|e|^2 - \mathrm{Re}\,(eV_i^*)) \\ -\mathrm{Im}\,(eV_i^*) \end{bmatrix} \quad (8)$$

where V_i is the voltage vector, and $i = 0,1,2\ldots 6$. The voltage vector corresponding to the i-th switching state, $[V_{i\alpha}, V_{i\beta}]$, can be derived as

$$\begin{bmatrix} V_{i\alpha} \\ V_{i\beta} \end{bmatrix} = \frac{2}{3}V_{dc}\begin{bmatrix} S_{ia} - \frac{1}{2}(S_{ib} + S_{ic}) \\ \frac{\sqrt{3}}{2}(S_{ib} - S_{ic}) \end{bmatrix} \quad (9)$$

where S_{ia}, S_{ib} and S_{ic} are the converter switching states, and V_{dc} is the DC-bus voltage.

Assume the tracking error of the DC-bus voltage to be constant during two sampling periods. The instant power at the beginning of the following $(k + 1)$-th sampling instant can be evaluated by linear extrapolation, and the corresponding

predicted active and reactive powers of the converter switching state can be derived as:

$$\begin{bmatrix} P_i^{k+1} \\ Q_i^{k+1} \end{bmatrix} = T_s\left(-\frac{R}{L}\begin{bmatrix} P_i^k \\ Q_i^k \end{bmatrix} + \omega\begin{bmatrix} -Q_i^k \\ P_i^k \end{bmatrix} \right.$$
$$\left. + \frac{3}{2L}\begin{bmatrix} (|e|^2 - \mathrm{Re}\,(eV_i^*)) \\ -\mathrm{Im}\,(eV_i^*) \end{bmatrix} \right) + \begin{bmatrix} P_i^k \\ Q_i^k \end{bmatrix} \quad (10)$$

where T_s is the sampling period. For the conventional dual-vector-based MPDCC, the P and Q differences between the references, P^{ref} and Q^{ref}, and predictive values, P_i^{k+1} and Q_i^{k+1}, of the i-th switching state with non-zero voltage vector, V_i, at the $(k + 1)$-th sampling instant are evaluated by a predefined cost function

$$j_i = (P^{ref} - P_i^{k+1})^2 + (Q^{ref} - Q_i^{k+1})^2 \quad (11)$$

and the non-zero voltage vector is pick as the optimal one if it yields a minimum cost function value.

Assuming the power slopes are kept constant during quite a small sampling period, one can predict the active and reactive powers at the end of a control period by

$$\begin{cases} P^{k+1} = P^k + \delta_{pn}t_n + \delta_{pz}t_z \\ Q^{k+1} = Q^k + \delta_{qn}t_n + \delta_{qz}t_z \end{cases} \quad (12)$$

where δ_{pn} and δ_{pz} are the P slopes of the non-zero voltage vectors, V_n, and zero voltage vector, V_z; δ_{qn} and δ_{qz} the Q slopes; t_n and t_z the durations of V_n and V_z, respectively, and $t_n + t_z = T_s$.

The errors between the predicted and reference power values can be derived as

$$\begin{cases} P_{err} = P^{ref} - \left(P^k + \delta_{pn}t_n + \delta_{pz}t_z\right) \\ Q_{err} = Q^{ref} - \left(Q^k + \delta_{qn}t_n + \delta_{qz}t_z\right) \end{cases} \quad (13)$$

where P_{err} and Q_{err} are the power errors, and P^{ref} and Q^{ref} are the reference power, respectively. The optimal durations can then be calculated by using the least-square optimization method [28]–[31] to minimize the cost function of power errors defined as

$$\begin{cases} J = P_{err}^2 + Q_{err}^2 \\ \frac{\partial J}{\partial t_n} = 0 \end{cases} \quad (14)$$

Finally, the optimal durations can be derived as

$$\begin{cases} t_n = \frac{(P^{ref} - P^k)(\delta_{pn} - \delta_{pz}) + (Q^{ref} - Q^k)(\delta_{qn} - \delta_{qz})}{(\delta_{pn} - \delta_{pz})^2 + (\delta_{qn} - \delta_{qz})^2} \\ \qquad + \frac{T_s(\delta_{pz}^2 + \delta_{qz}^2 - \delta_{pn}\delta_{pz} - \delta_{qn}\delta_{qz})}{(\delta_{pn} - \delta_{pz})^2 + (\delta_{qn} - \delta_{qz})^2} \\ t_z = T_s - t_n \end{cases} \quad (15)$$

Once t_n and t_z are calculated, the pulse width modulation (PWM) switching signals can be generated at a fixed switching frequency. However, the duration based on (15) could be negative or over T_s, especially at a dynamic instant with large instantaneous active or reactive power error. The measure is to force the action time to zero whenever the negative duration

exists and saturate the other duration to T_s, which may lead to steady state performance deterioration or dynamic power overshoot. The hardware with high computing capability is required for the calculation of power slopes and optimal durations.

IV. SIMPLIFIED PREDICTIVE DIRECT DUTY-CYCLE-CONTROL

To solve the issues mentioned above, this paper proposes the SPDDC, which differs from the MPDPC by just adding one more step of the duty-cycle calculation. By emulating the implementation of SVM, the proposed method assigns a portion of the control period directly in reciprocal proportional with the cost function value of corresponding optimal dual vectors, which means the cost function is not only used for the best vector selection but also applied for duration calculation. Thus, it can eliminate the power slope calculation of each vector as in (12), which is more intuitive compared with the MPDCC while retaining the fixed-switching frequency feature. Besides, the negative duration issue of MPDCC is essentially resolved. Merits of both the MPDPC and MPDCC are retained.

A. PRINCIPLE OF THE PROPOSED SPDDC

Based on the cost function

$$J_i = (P^* - P_i^{k+1})^2 + (Q^* - Q_i^{k+1})^2 \qquad (16)$$

the best non-zero vector, V_i, yielding the minimum J_i is selected. The cost function can also be defined in the abstract form as

$$J_i = \left| P^{ref} - P_i^{k+1} \right| + \left| Q^{ref} - Q_i^{k+1} \right| \qquad (17)$$

though they do not have noticeable differences [16].

The duration can then be directly derived from the inverse proportion to the cost function results of the selected dual vectors, which further takes full use of the cost function values, as

$$\begin{cases} \dfrac{k}{J_i} + \dfrac{k}{\lambda J_0} = T_s \\ t_n = k\dfrac{1}{J_i} \qquad t_z = k\dfrac{1}{\lambda J_0} \end{cases} \qquad (18)$$

where k is the gain for duration calculation and can be solved easily, J_0 the cost function value of the zero vector, λ an added parameter to balance the ratio of J_0 and J_i, which will be verified in the following subsection, and t_n and t_z are the duration of the non-zero vector and zero vector, respectively, which are all positive. Usually, λ can be selected in the range between 1 and 2 to achieve better steady state and dynamic performance simultaneously.

According to (18), the corresponding duty cycles for dual vectors can be calculated by

$$\begin{cases} d_n = \dfrac{\lambda J_0}{J_i + \lambda J_0} \qquad t_n = d_n T_s \\ d_z = \dfrac{J_i}{J_i + \lambda J_0} \qquad t_z = d_z T_s \end{cases} \qquad (19)$$

where d_n and d_z are the duty cycles of non-zero vector V_n and zero vector V_z. If $J_i/\lambda J_0$ decreases, d_n would increase, meaning the best active vector constitutes an increased proportion of the control period. Otherwise, the zero vector would constitute an increased proportion of the control period. The balanced modulation scheme can adjust the duty cycle automatically.

Different to the MPDCC, the durations are simply calculated by (18) rather than (15) and directly allocated to the corresponding vectors. The calculations of power slopes for each vector are eliminated, which reduces the calculation burden and is intuitive for implementation. Since t_n and t_z are undoubtedly within the range of 0 to T_s in inverse proportion to J_i and λJ_0, respectively, it can eliminate the need of compensation, and the negative duration issue is essentially solved. Table 1 compares the complexities of MPDCC, SPDDC, and MPDPC.

TABLE 1. Complexity comparisons of each control scheme.

Control Requirement	MPDCC	SPDDC	MPDPC
Cost function	Need	Need	Need
Slope of *P&Q*	Need	No need	No need
Least-square optimization	Need	No need	No need
Duration equation (complexity)	High	Low	No need
Compensation measure	Need	No need	No need
PWM Signal	Need	Need	No need

B. MATHEMATICAL ANALYSIS OF THE PROPOSED SPDDC

Using complex apparent power, (8) can be rewritten as

$$\frac{dS}{dt} = \frac{1}{L}\left[-(R - j\omega L)\cdot S + \frac{3}{2}\left(|\bar{e}|^2 - \bar{V}^*\bar{e}\right)\right] \qquad (20)$$

where S is the complex power from the power grid.

Thus, the slope of the negative conjugate of complex apparent power in the synchronous dq frame, denoted as $-S^*$, can be derived as

$$\frac{d(-S^*)}{dt} = \frac{1}{L}\left[(R + j\omega L)\cdot S^* - \frac{3}{2}E^2 + \frac{3}{2}Ev_{dq}\right] \qquad (21)$$

where E and v_{dq} are the amplitudes of grid *emf* vector e and terminal voltage vector V. Since the complex apparent power is irrelevant to the transformation frame, the subscript "*dq*" of $-S^*$ is neglected.

In terms of the apparent power, the cost function (17) can be rewritten as

$$G = \left| S^{ref} - S^{k+1} \right| = \left| (-S^*)^{ref} - (-S^*)^{k+1} \right| \qquad (22)$$

where the superscript "ref" stands for reference, $k + 1$ denotes the predictive value for the next control period.

The predicted value $(-S^*)^{k+1}$ can be derived from (21) as

$$(-S^*)^{k+1} = \underbrace{(-S^*)^k + \frac{T_s}{L}\left[(R+j\omega L)\cdot(S^*)^k - \frac{3}{2}E^2\right]}_{(-S^*)_0^{k+1}}$$

$$+ \frac{3ET_s}{2L}v_{dq} \quad (23)$$

According to (23), the cost function in (22) can be rearranged as

$$G = \left|\Delta(-S^*)_0^{k+1} - \frac{3ET_s}{2L}v_{dq}\right| \quad (24)$$

where $\Delta(-S^*)_0^{k+1} = (-S^*)^{ref} - (-S^*)_0^{k+1}$ represents the error vector caused by the zero voltage vector.
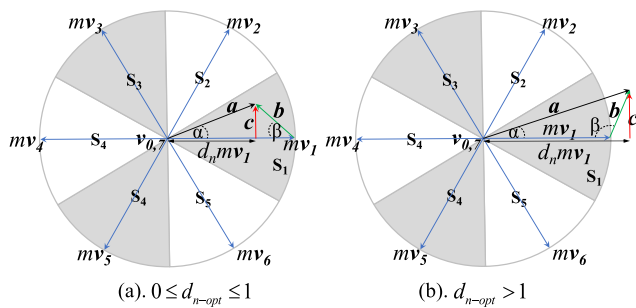

(a). $0 \le d_{n-opt} \le 1$ (b). $d_{n-opt} > 1$

FIGURE 2. Principle of calculating duty cycle d_{n-opt} of optimized non-zero vector in a synchronous frame, where $a = \Delta(-S^*)_0^{k+1}$, $b = \Delta(-S^*)_0^{k+1} - mv_1$, and $m = 1.5ET_s/2L$.

As shown in Fig. 2, the cost function error G_0 caused by the zero vector, namely $a = \Delta(-S^*)_0^{k+1}$, is supposed to be located in sector S_1. The non-zero vector closest to a is the best one that can minimize the cost function in (24). Thus, v_1 would be selected and $0° \le \alpha \le 30°$. Based on (24), the error G_1 caused by v_1 can be illustrated as vector b in Fig. 2, where $m\, v_1$ indicates the second term of (23), $m = 1.5ET_s/2L$. The combined error vector c caused by the zero vector and v_1 with non-zero vector duty cycle d_n can then be derived as

$$c = d_n b + (1-d_n)a = d_n(a - mv_1)$$
$$+ (1-d_n)a = a - d_n mv_1 \quad (25)$$

To minimize the combined error, vector c should be perpendicular to $m\, v_1$, as illustrated in Fig. 2. Finally, the optimized duty cycle d_{n-opt} can be obtained by

$$d_{n-opt} = \frac{|a|\cos\alpha}{m|v_1|} = \frac{|a|\cos\alpha}{|a|\cos\alpha + |b|\cos\beta}$$
$$= \frac{|a|}{|a| + |b|\frac{\cos\beta}{\cos\alpha}} \quad (26)$$

According to (26), d_{n-opt} can be greater than 1 if $\beta > 90°$, especially at a dynamic instant with large instant power error, as illustrated in Fig. 2(b). In a real control system, $0 \le d_{n-opt} \le 1$ should be forced.

Therefore, the SPDCC with (19) can be rearranged as

$$d_n = \frac{\lambda G_0}{\lambda G_0 + G_1} = \frac{|a|}{\lambda|a| + |b|} = \frac{|a|}{|a| + |b|\frac{1}{\lambda}} \quad (27)$$

By replacing $\cos\alpha/\cos\beta$ with λ, the calculation complexity can be significantly reduced.

In the steady state, generally, both the zero vector and best non-zero vector are selected for implementation, which means $0 \le d_{n-opt} \le 1$ and $0° \le \beta \le 90°$. Since d_{n-opt} has a large chance to be in the middle range between 0 and 1, we can assume that $0° \le \beta \le 60°$ in most cases. Also, it is reasonable to suppose that generally the active vector error b has a lower value than the zero vector error a, namely $\alpha < \beta$, since the active vector is selected instead of the zero vector in most cases with single-vector-based methods, such as STDPC and MPDPC. Based on the assumption $0° \le \beta \le 60°$ and $\alpha < \beta$, as $0° \le \alpha \le 30°$ and $\lambda = \cos\alpha/\cos\beta$, it can be deduced that $1 \le \lambda \le 2$ in general. This has also been verified through trial and error in simulations and experiments.

Since the complex mathematical calculation is no longer needed and λ theoretically equals to $\cos\alpha/\cos\beta$, it is impossible to give the exact range of the λ. The above analyses about λ are just based on a reasonable assumption and derivation. In some special cases, λ could be out the range mentioned above. Through the numerical simulation and experimental tests presented in sections V and VI, it has been verified that the control method works well if λ is in the range of 1 and 2 in the steady state, though the dynamic performance is influenced a lot by the choice of λ. At the beginning of design, the value of λ can be optimized for good dynamic performance by simulation in MATLAB/Simulink in the range of 1 and 2. It can then be adjusted slightly and applied in experiments.

C. VECTOR SEQUENCE FOR SWITCHING FREQUENCY OPTIMIZATION

In regard to the vector sequence to realize the minimal commutation between vectors in an application, two aspects about vector sequence should comply in order. Firstly, if the vector sequence during the previous cycle is with the zero vector at the end, the same zero vector should be selected and applied first in the next cycle to reduce the switching commutation. Otherwise, the sequence of non-zero vector and zero vector should be changed in order to achieve the minimal commutation between the current and the previous vector sequences. Meanwhile, the proper zero vector that requires the least commutation of the current vector sequence should be selected.

For example, if active vector "100" is chosen to implement and the last vector of the previous sequence is "010," the proper zero vector will be "000" instead of "111," and the vector applied firstly should be "000" rather than "100," as it has only two commutations rather than three. By realizing the fixed switching frequency, the switching frequency can be reduced to a certain degree.

D. DESIGN OF ONE-STEP-DELAY COMPENSATION

The one-step-delay between the commanding voltage vector and the applied voltage vector caused by the discrete-time digital implementation can significantly deteriorate the control performance, such as power control performance and power prediction error [8], [19]. Thus, the one-step-ahead prediction is required during implementation of SPDDC.

Firstly, the combined voltage V is built with currently implemented vectors and durations as

$$V = V_n d_n + V_z d_z \tag{28}$$

Substituting (28) into (10), one can obtain the predicted values of P^{k+1} and Q^{k+1} at the $(k + 1)$-th instant with V.

Based on P^{k+1} and Q^{k+1}, the one-step-ahead prediction P_i^{k+2} and Q_i^{k+2} of each active vector can be calculated for the next best vector selection by

$$\begin{bmatrix} P_i^{k+2} \\ Q_i^{k+2} \end{bmatrix} = T_s \left(-\frac{R}{L} \begin{bmatrix} P^{k+1} \\ Q^{k+1} \end{bmatrix} + \omega \begin{bmatrix} -Q^{k+1} \\ P^{k+1} \end{bmatrix} \right.$$
$$\left. + \frac{3}{2L} \begin{bmatrix} (|e|^2 - \mathrm{Re}\left(eV_i^*\right)) \\ -\mathrm{Im}\left(eV_i^*\right) \end{bmatrix} \right) + \begin{bmatrix} P^{k+1} \\ Q^{k+1} \end{bmatrix} \tag{29}$$

The cost function (17) can be revised as

$$J_i = \left| P^* - P_i^{k+2} \right| + \left| Q^* - Q_i^{k+2} \right| \tag{30}$$

The duration for each vector can still be calculated by (19). Fig.3 illustrates schematically the block diagram of the proposed SPDDC.
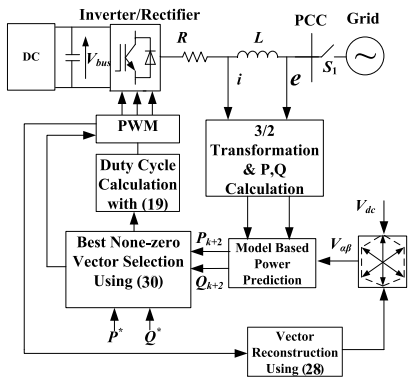

FIGURE 3. Block diagram of SPDDC for grid-connected AC/DC converter.

V. NUMERICAL SIMULATION

The performance of proposed SPDDC has been simulated in MATLAB/Simulink, and compared with the performances of the conventional single-vector-based MPDPC and the dual-vector-based MPDCC. The one-step-delay compensation is applied to the model-predictive-based control methods during the procedure of the best vector selection by using equations similar to (29) and (30). The power flow from the AC side to the DC load is defined as positive. Table 2 lists the power circuit parameters, and the sampling frequency is 20 kHz.

TABLE 2. Electrical parameter of the power circuit.

Resistance of reactor	R	510 mΩ
Inductance of reactor	L	4 mH
DC-bus capacitor	C	680 uF
Load resistance	R_L	34 Ω
Source voltage	e	36 V(peak)
Source voltage frequency	f	50 Hz
DC-bus voltage	V_{dc}	120 V

A. STEADY STATE PERFORMANCE COMPARISON

For the steady state performance comparison, the AC three-phase voltage, current, and instantaneous active and reactive powers of the system under each of the above three control methods are depicted, where the reactive power reference is set as 200 VAR and the active power reference as 400 W. As shown in Fig. 4, both the active and reactive powers can track the reference values with high accuracy.

Fig. 4(a) shows that under the MPDPC method, the system exhibits high P and Q ripples of 11.05 W and 12.32 VAR, respectively, and a current total harmonic distortion (THD) of 3.77%. On the other hand, the dual-vector-based methods can achieve much better results than the MPDPC method. For instance, under the control of MPDCC method, as shown in Fig. 4(b), the system exhibits a current THD of 1.49%, and P and Q ripples of 4.87 W and 4.27 VAR, respectively, which are less than half of those under the MPDPC method.

Under the control of proposed SPDDC, while the steady state performance is very close to that of MPDCC method, there exists some small difference. For instance, compared with MPDCC, the Q ripple is further reduced to 3.98 VAR, and the current THD 1.43%, but the P ripple is 5.12 W when $\lambda = 1$, which is slightly higher than that of MPDCC. When $\lambda = 1.5$, the steady state performance is not far away from that when $\lambda = 1$ with slightly increased Q ripple and THD. Table 3 compares quantitatively the performance indicators of the above three control methods, such as the current THD and active and reactive power ripples in different states ($P = 400$ W, $Q = 0$ VAR). As shown, the MPDPC method yields the highest current THD with a wide harmonic spectrum. On the other hand, the proposed SPDDC method yields a slightly better current THD with much lower low-order harmonic contents than those of the MPDCC. The current harmonics of the MPDCC and SPDDC methods concentrate at 20 kHz, which is a common feature of dual-vector-based control and can result in much simpler filter design. In conclusion, the proposed SPDDC can achieve a steady state performance much better than that of the MPDPC method and a steady state performance comparable to that of the MPDCC method.

B. DYNAMIC PERFORMANCE COMPARISON

The dynamic performances of these control methods under the same step power change references are compared. As illustrated in Fig. 5, the active and reactive power references are set as 400 W and 0 VAR, respectively, from 0 s. At 0.02 s, the P reference drops to 100 W, and at 0.03 s,
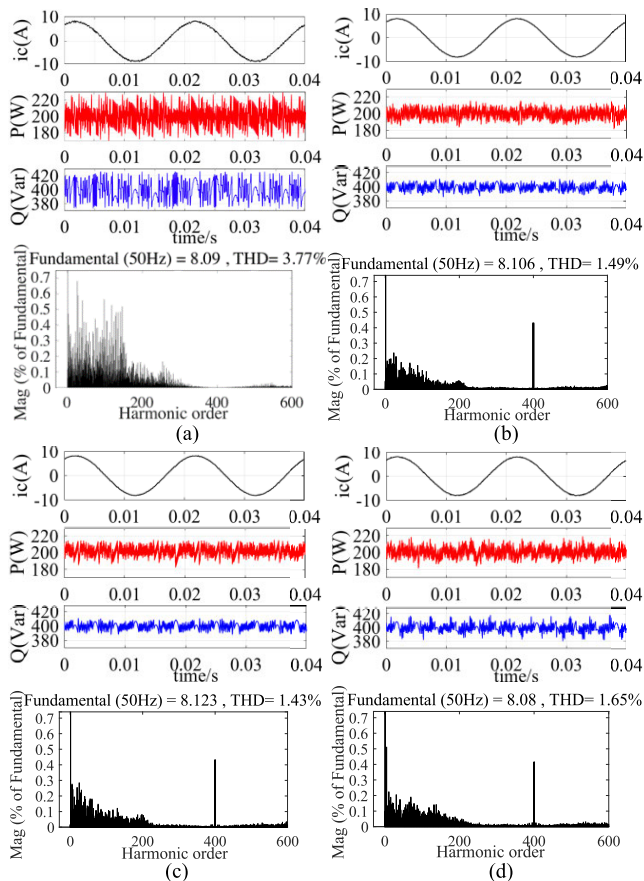
FIGURE 4. Steady state performance at P = 200 W, Q = 400 VAR. Top to bottom: i_c, P, Q, and harmonic spectrum of i_c. (a). MPDPC. (b). MPDCC. (c). SPDDC-1 (λ = 1). (d). SPDDC-1.5 (λ = 1.5).

TABLE 3. Quantitative comparison of simulation results.

Control	P=200W Q=400VAR			P=400W Q=0VAR			
	THD (%)	Prip (W)	Qrip (VAR)	THD (%)	Prip (W)	Qrip (VAR)	Response Time(s)
MPDPC	3.77	11.1	12.3	3.91	9.94	11.9	0.0008
MPDCC	1.49	4.87	4.27	1.93	5.37	5.47	0.0007
SPDDC-1	1.43	5.12	3.98	1.97	6.3	5.1	0.0039
SPDDC-1.5	1.65	5.3	5.28	1.99	6.25	5.29	0. 0014

TABLE 4. Electrical parameter of prototype.

Resistance of reactor	R	500mΩ
Inductance of reactor	L	22 mH
DC-bus capacitor	C	680 uF
Load resistance	R_L	34 Ω
Source line voltage	e	60 V
Source voltage frequency	f	50 Hz

The parameters are listed in Table 4. The power circuit was controlled by a TMS320F28335 floating-point digital signal processor (DSP) based on Texas Instruments (TI) C2000 target board for A/D sampling, PWM signal generation and D/A output. The variables such as the reference value changes are controlled by the real-time data exchange communication between the DSP and PC.

A. COMPARISON OF STEADY STATE PERFORMANCE

For each of the three control methods, the current THD, P and Q ripples at P = 200 W and Q = 400 VAR have been recorded at the sampling frequency of 10 kHz except where specialized. The MPDPC with a sampling frequency of 20 kHz and three-vector-based predictive duty-cycle-control (TPDCC) with an additional vector sequence in [25] are also implemented for comparison. Among various three-vector predictive control methods, TPDCC is one of the most popular and known methods. For simplicity, the MPDPC control with 10 kHz and 20 kHz sampling frequency are indicated as MPDPC-10kHz and MPDPC-20kHz, and the SPDDC method with λ = 1 and λ = 1.5 as SPDDC-1 and SPDDC-1.5, respectively. One-step-delay compensation is applied to each of the control methods. Among various predictive control methods, these above mentioned are the most popular and known methods. While for comparisons, due to the page limit, the comparisons of eight different control methods including the single-vector-based, dual-vector-based, and three-vector-based methods are presented in [37].

Fig. 7(a) shows the PWM driving signal of the upper switch of phase A, input phase to phase voltage V_{ab}, and input current i_a and i_b of the MPDPC method with 10 kHz sampling frequency. The PWM signals are input signals, while V_{ab}, i_a and i_b shown on the oscilloscope are output signals. Also, with the experimental data acquired from the oscilloscope to PC, the instantaneous P and Q, harmonic spectrum analyses of i_a are presented. The current THD is 4.95% as shown by the harmonic spectrum of i_a. The active and reactive power tracks the references very well. The P and Q ripples are 19.55 W and 22.88 VAR, respectively.

the Q reference drops to −300 VAR. Then, at 0.04 s, the active power reference steps up to 800 W, and at 0.06 s, the reactive power reference drops to −400 VAR. Finally, at 0.11 s, the P reference is reduced to 200 W.

As shown, the dynamic response of every control method can track the reference values of P and Q with high accuracy and stability. Under the control of either MPDPC or MPDCC method, an overshoot of P appears at the instant of Q step change. Under the control of proposed SPDDC, when λ = 1, the dynamic response to a step change of P reference at 0.02 s is much slower than those of the MPDPC and MPDCC. However, when λ = 1.5, as shown in Fig. 5(d), the overshoot almost disappeared, indicating a good dynamic performance with rapid dynamic response and accurate reference tracking ability. This is also shown in the quantitative comparison of instantaneous states presented in Table 3.

In conclusion, the proposed SPDDC method is an effective and intuitive method with better steady state and dynamic performance than those of the MPDPC method, and it can be simply transformed from the MPDPC method.

VI. EXPERIMENTAL TESTS

To verify the effectiveness of the proposed SPDDC method, a scaled-down prototype is built as shown in Fig. 6.
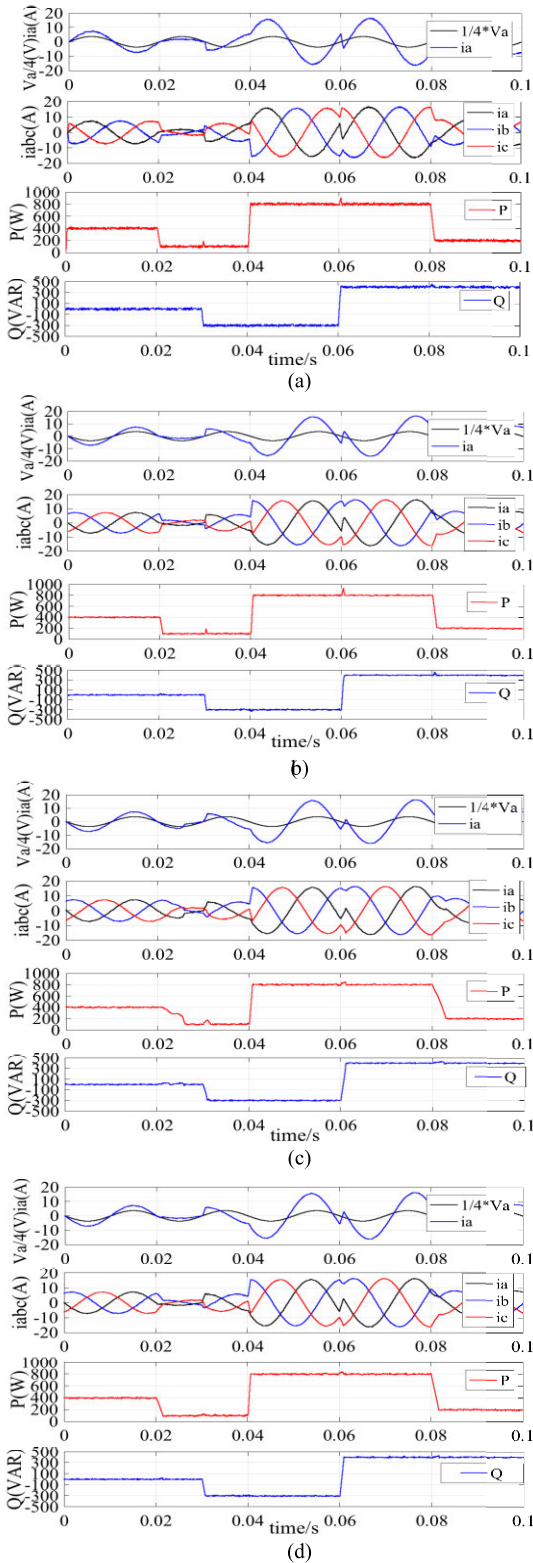
FIGURE 5. Dynamic-state performance with bi-directional power flow. Top to bottom: V_a and i_a, three-phase current, P and Q. (a). MPDPC. (b). MPDCC. (c). SPDDC-1 ($\lambda = 1$). (d). SPDDC-1.5 ($\lambda = 1.5$).
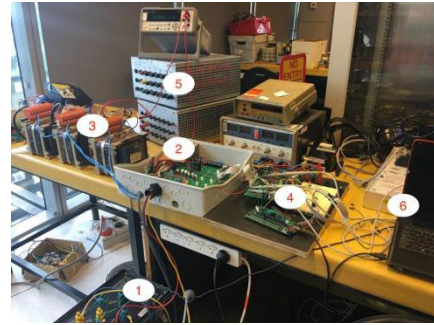
FIGURE 6. Experimental setup of three-phase AC/DC converter, (1) Three-phase isolated transformer, (2) Main circuit of the converter, (3) Inductors, (4) TI C2000 target and interface board (5) DC resistive load, and (6) PC.

TABLE 5. Quantitative comparison of steady states.

Control	fs (Hz)	THD (%)	Prip (W)	Qrip (VAR)
MPDPC-10kHz	10 K	4.95	19.55	22.88
MPDPC-20kHz	20 K	3.54	16.74	17.77
TPDCC	10 K	3.71	17.18	16.26
MPDCC	10K	4.00	17.49	19.52
SPDDC-1	10 K	3.73	18.23	18.52
SPDDC-1.5	10 K	3.70	19.21	18.34

burden on hardware and increased switching frequency. With MPDPC-20kHz, the current THD is reduced to 3.54%, the active and reactive power ripples are also decreased obviously as presented in Table 5.

As shown in Fig. 7(c), the steady state performance of TPDCC with 10 kHz sampling frequency is close to that of MPDPC-20kHz, showing that the multi-vector-based control method can perform much better than the single-vector-based control method.

The steady state performance of the MPDCC in Fig. 7(d) shows a slight deterioration in comparison to that of TPDCC due to the application of dual-vectors, but it is still better than that of the single-vector-based MPDPC-10kHz method. The performances of the proposed SPDDC-1 and SPDDC-1.5 methods are presented in Fig. 7(e) and Fig. 7(f), respectively. As shown, they both can achieve slightly lower current THD and Q ripples compared with the MPDCC, though the P ripple is increased. It is confirmed that the proposed method is superior to the MPDPC method and has comparable performance to the MPDCC method. As shown in Table 5, the experimental results agree well with the numerical simulation results. It should be noted that the deviations between the simulated and experimental results are mainly caused by the difference of sampling frequency.

The harmonic analysis shows that under the control of the proposed SPDDC, a significant proportion of the low-order harmonics is reduced in contrast to the MPDPC, which has a high proportion of low-order harmonics and a wide harmonic spectrum. Therefore, using the SPDDC method can reduce the complexity of filter design.

In comparison, the performance is enhanced a lot with MPDPC-20kHz as shown in Fig. 7(b), since the sampling frequency is increased with a heavier computational
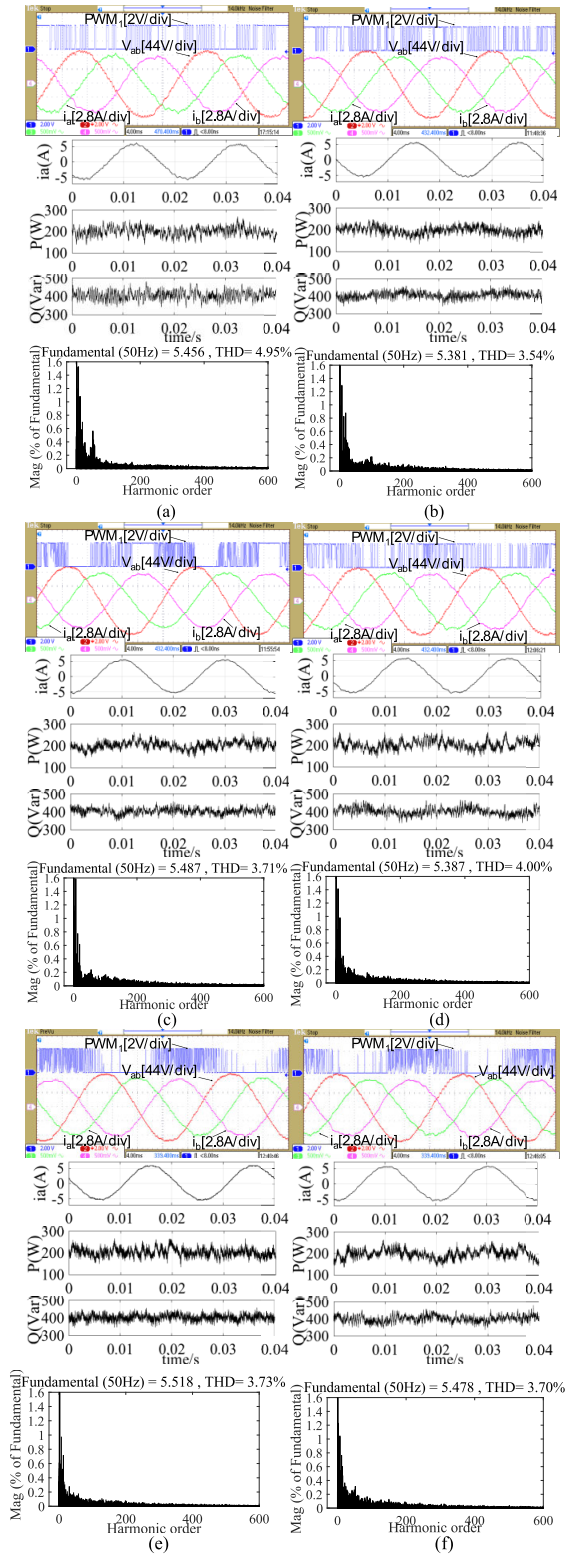
FIGURE 7. Steady state performance at *P* = 200 W, *Q* = 400 VAR. Top to bottom: Oscilloscope screenshot, *P*, *Q*, and harmonic spectrum of *iₐ*. (a) MPDPC-10kHz. (b) MPDPC-20kHz. (c) TPDCC. (d) MPDCC. (e) SPDDC-1. (f) SPDDC-1.5.

FIGURE 8. Dynamic-state performance when *P* varying from 200 W to 400 W, *Q* = 200 VAR. Top: Oscilloscope screenshot. Bottom: *iₐ*, *P* and *Q*. (a) MPDPC-10kHz, (b) MPDPC-20kHz, (c) TPDCC, (d) MPDCC, (e) SPDDC-1, and (f) SPDDC-1.5.

B. COMPARISON OF DYNAMIC PERFORMANCE

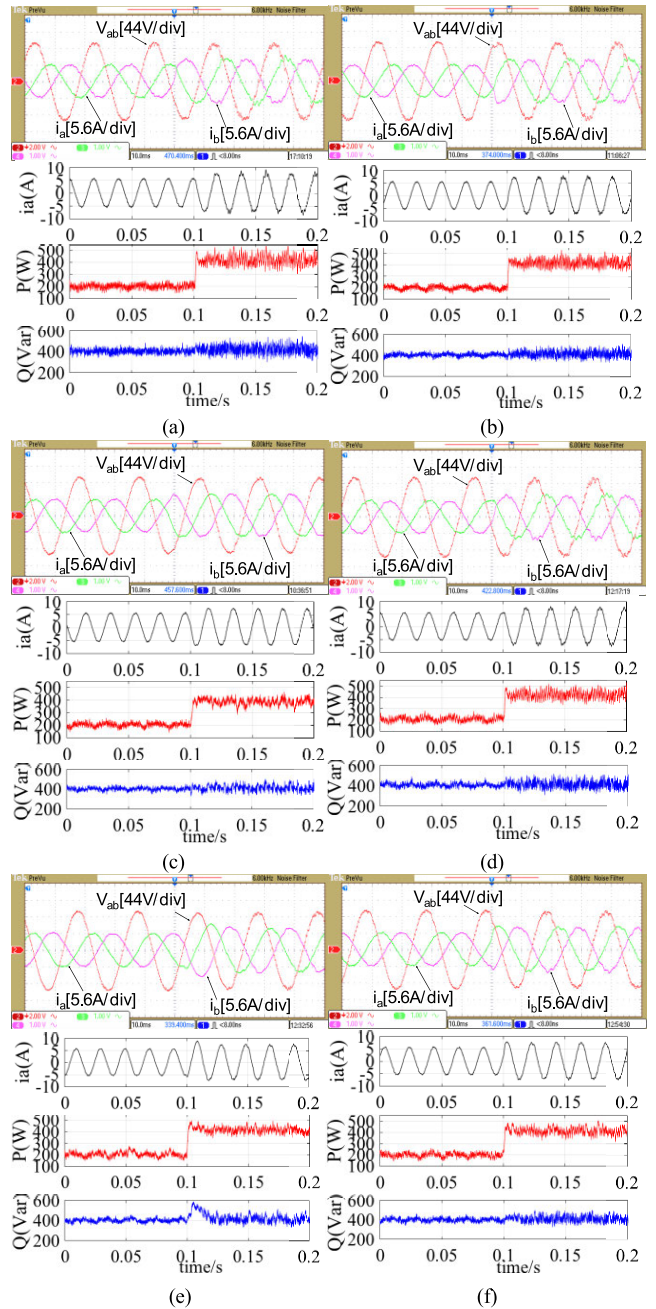Fig. 8 compares the experimental dynamic performance when the *P* reference increases from 200 W to 400 W, while the *Q* reference remains at 400 VAR. As shown, all control methods can follow the references accurately with similar response times. Fig. 8(f) shows that the SPDDC-1's dynamic response of reactive power is a bit slower than that of the SPDDC-1.5 method when the *P* reference has a step change. This agrees with the numerical simulation results.

C. SYSTEM PARAMETER REDUNDANCY

The robustness of the proposed SPDDC is examined through a series of experiments by setting the line inductance in
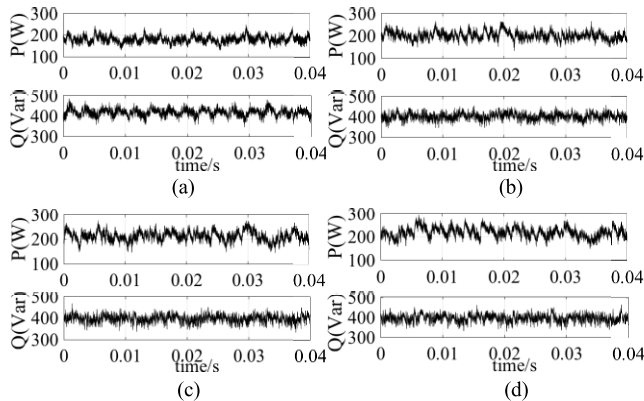
FIGURE 9. Responses of active and reactive power for proposed SPDDC when the actual inductance in control differs from the real value. (a) 10 mH, (b) 20 mH, (c) 30 mH, and (d) 40 mH.

the algorithm different from the actual value. As shown in Fig. 9(a), when the inductance set in SPDDC is 50% of the actual value (20 mH), the *Q* ripple increases and a negative DC offset of *P* appears. As shown in Figs. 9(c) and (d), the increase of inductance value used in the control algorithm to 30 mH and 40 mH has almost no influence on the *Q* ripple and positive DC offset of *P*. As confirmed by the experiments, under the control of proposed SPDDC, the precision of inductance, in a range of 50% to 200% of the actual value, has little influence on the steady state performance and control stability, which is superior to the MPDPC method [27].

VII. CONCLUSION

A simplified dual-vector-based SPDDC strategy for three-phase AC/DC converters is proposed in this paper to eliminate the time consuming procedure of duty-cycle optimization. In SPDCC, the cost function is used for both best vector selection and duration derivation. Compared with MPDPC, since dual vectors are implemented in each control session, SPDDC can achieve much better performance with a fixed switching frequency. Compared with MPDCC, SPDDC is more intuitive. The deduced value of duration is guaranteed to be within a definite range, and thus the issue of negative duration is essentially resolved. The procedure of duty-cycle optimization can be eliminated by the simplified calculation. The vector sequence optimization and one-step-delay compensation are considered in the proposed method.

The proposed SPDDC is compared comprehensively with various kinds of typical multi-vector-based control methods through numerical simulations and experimental tests. The correctness and effectiveness of the proposed SPDDC are validated by the results through superior steady state and dynamic performances with fixed switching frequencies, lower current THD, and lower active and reactive power ripples.

REFERENCES

[1] J. R. Rodriguez, J. W. Dixon, J. R. Espinoza, J. Pontt, and P. Lezana, "PWM regenerative rectifiers: State of the art," *IEEE Trans. Ind. Electron.*, vol. 52, no. 1, pp. 5–22, Feb. 2005.

[2] T. Geyer and D. E. Quevedo, "Multistep finite control set model predictive control for power electronics," *IEEE Trans. Power Electron.*, vol. 29, no. 12, pp. 6836–6846, Dec. 2014.

[3] S. Chakraborty, B. Kramer, and B. Kroposki, "A review of power electronics interfaces for distributed energy systems towards achieving low-cost modular design," *Renew. Sustain. Energy Rev.*, vol. 13, no. 9, pp. 2323–2335, Dec. 2009.

[4] N. Flourentzou, V. G. Agelidis, and G. D. Demetriades, "VSC-based HVDC power transmission systems: An overview," *IEEE Trans. Power Electron.*, vol. 24, no. 3, pp. 592–602, Mar. 2009.

[5] A. Rahoui, A. Bechouche, H. Seddiki, and D. O. Abdeslam, "Grid voltages estimation for three-phase PWM rectifiers control without AC voltage sensors," *IEEE Trans. Power Electron.*, vol. 33, no. 1, pp. 859–875, Jan. 2018.

[6] Y. Zhang, J. Gao, and C. Qu, "Relationship between two direct power control methods for PWM rectifiers under unbalanced network," *IEEE Trans. Power Electron.*, vol. 32, no. 5, pp. 4084–4094, May 2017.

[7] Y. Zhang and C. Qu, "Table-based direct power control for three-phase AC/DC converters under unbalanced grid voltages," *IEEE Trans. Power Electron.*, vol. 30, no. 12, pp. 7090–7099, Dec. 2015.

[8] J. Hu, J. Zhu, and D. G. Dorrell, "In-depth study of direct power control strategies for power converters," *IET Power Electron.*, vol. 7, no. 7, pp. 1810–1820, Jul. 2014.

[9] J. Alonso-Martínez, J. E. Carrasco, and S. Arnaltes, "Table-based direct power control: A critical review for microgrid applications," *IEEE Trans. Power Electron.*, vol. 25, no. 12, pp. 2949–2961, Dec. 2010.

[10] W. Xiong, Y. Sun, J. Lin, M. Su, H. Dan, M. Rivera, and J. M. Guerrero, "A cost-effective and low-complexity predictive control for matrix converters under unbalanced grid voltage conditions," *IEEE Access*, vol. 7, pp. 43895–43905, 2019.

[11] A. Bouafia, F. Krim, and J.-P. Gaubert, "Fuzzy-Logic-Based switching state selection for direct power control of three-phase PWM rectifier," *IEEE Trans. Ind. Electron.*, vol. 56, no. 6, pp. 1984–1992, Jun. 2009.

[12] A. Bouafia, J.-P. Gaubert, and F. Krim, "Predictive direct power control of three-phase pulsewidth modulation (PWM) rectifier using space-vector modulation (SVM)," *IEEE Trans. Power Electron.*, vol. 25, no. 1, pp. 228–236, Jan. 2010.

[13] S. Vazquez, J. Rodriguez, M. Rivera, L. G. Franquelo, and M. Norambuena, "Model predictive control for power converters and drives: Advances and trends," *IEEE Trans. Ind. Electron.*, vol. 64, no. 2, pp. 935–947, Feb. 2017.

[14] Y. Cho and K.-B. Lee, "Virtual-Flux-Based predictive direct power control of three-phase PWM rectifiers with fast dynamic response," *IEEE Trans. Power Electron.*, vol. 31, no. 4, pp. 3348–3359, Apr. 2016.

[15] J. Liu, S. Vazquez, L. Wu, A. Marquez, H. Gao, and L. G. Franquelo, "Extended state observer-based sliding-mode control for three-phase power converters," *IEEE Trans. Ind. Electron.*, vol. 64, no. 1, pp. 22–31, Jan. 2017.

[16] S. Kouro, P. Cortes, R. Vargas, U. Ammann, and J. Rodriguez, "Model predictive control—A simple and powerful method to control power converters," *IEEE Trans. Ind. Electron.*, vol. 56, no. 6, pp. 1826–1838, Jun. 2009.

[17] S. Vazquez, J. I. Leon, L. G. Franquelo, J. Rodriguez, H. A. Young, A. Marquez, and P. Zanchetta, "Model predictive control: A review of its applications in power electronics," *IEEE Ind. Electron. Mag.*, vol. 8, no. 1, pp. 16–31, Mar. 2014.

[18] B. Stellato, T. Geyer, and P. J. Goulart, "High-speed finite control set model predictive control for power electronics," *IEEE Trans. Power Electron.*, vol. 32, no. 5, pp. 4007–4020, May 2017.

[19] Y. Zhang and W. Xie, "Low complexity model predictive Control—Single vector-based approach," *IEEE Trans. Power Electron.*, vol. 29, no. 10, pp. 5532–5541, Oct. 2014.

[20] C. Xia, T. Liu, T. Shi, and Z. Song, "A simplified Finite-Control-Set model-predictive control for power converters," *IEEE Trans. Ind. Informat.*, vol. 10, no. 2, pp. 991–1002, May 2014.

[21] H. A. Young, M. A. Perez, and J. Rodriguez, "Analysis of Finite-Control-Set model predictive current control with model parameter mismatch in a three-phase inverter," *IEEE Trans. Ind. Electron.*, vol. 63, no. 5, pp. 3100–3107, May 2016.

[22] H. T. Nguyen, J. Kim, and J.-W. Jung, "Improved model predictive control by robust prediction and stability-constrained finite states for three-phase inverters with an output *LC* filter," *IEEE Access*, vol. 7, pp. 12673–12685, 2019.

[23] Y. Zhang, Y. Bai, and H. Yang, "A universal Multiple-Vector-Based model predictive control of induction motor drives," *IEEE Trans. Power Electron.*, vol. 33, no. 8, pp. 6957–6969, Aug. 2018.

[24] J. Hu and Z. Q. Zhu, "Investigation on switching patterns of direct power control strategies for grid-connected DC–AC converters based on power variation rates," *IEEE Trans. Power Electron.*, vol. 26, no. 12, pp. 3582–3598, Dec. 2011.

[25] J. Hu and Z. Q. Zhu, "Improved voltage-vector sequences on dead-beat predictive direct power control of reversible three-phase grid-connected voltage-source converters," *IEEE Trans. Power Electron.*, vol. 28, no. 1, pp. 254–267, Jan. 2013.

[26] S. Vazquez, A. Marquez, R. Aguilera, D. Quevedo, J. I. Leon, and L. G. Franquelo, "Predictive optimal switching sequence direct power control for grid-connected power converters," *IEEE Trans. Ind. Electron.*, vol. 62, no. 4, pp. 2010–2020, Apr. 2015.

[27] Z. Song, W. Chen, and C. Xia, "Predictive direct power control for three-phase grid-connected converters without sector information and voltage vector selection," *IEEE Trans. Power Electron.*, vol. 29, no. 10, pp. 5518–5531, Oct. 2014.

[28] Y. Zhang, W. Xie, Z. Li, and Y. Zhang, "Low-complexity model predictive power control: Double-Vector-Based approach," *IEEE Trans. Ind. Electron.*, vol. 61, no. 11, pp. 5871–5880, Nov. 2014.

[29] Z. Song, Y. Tian, W. Chen, Z. Zou, and Z. Chen, "Predictive duty cycle control of three-phase Active-Front-End rectifiers," *IEEE Trans. Power Electron.*, vol. 31, no. 1, pp. 698–710, Jan. 2016.

[30] Y. Zhang, W. Xie, Z. Li, and Y. Zhang, "Model predictive direct power control of a PWM rectifier with duty cycle optimization," *IEEE Trans. Power Electron.*, vol. 28, no. 11, pp. 5343–5351, Nov. 2013.

[31] Y. Zhang, Y. Peng, and H. Yang, "Performance improvement of Two-Vectors-Based model predictive control of PWM rectifier," *IEEE Trans. Power Electron.*, vol. 31, no. 8, pp. 6016–6030, Aug. 2016.

[32] L. Tarisciotti, J. Lei, A. Formentini, A. Trentin, P. Zanchetta, P. Wheeler, and M. Rivera, "Modulated predictive control for indirect matrix converter," *IEEE Trans. Ind. Appl.*, vol. 53, no. 5, pp. 4644–4654, Sep. 2017.

[33] X. Shi, J. Zhu, L. Li, D. D.-C. Lu, J. Zhang, and H. Yang, "Predictive duty cycle control with reversible vector selection for three-phase AC/DC converters," *IEEE Trans. Power Electron.*, vol. 34, no. 5, pp. 4868–4882, May 2019.

[34] Y. Zhang, J. Liu, H. Yang, and S. Fan, "New insights into model predictive control for three-phase power converters," *IEEE Trans. Ind. Appl.*, vol. 55, no. 2, pp. 1973–1982, Mar. 2019.

[35] S.-Y. Park and S. Kwak, "Comparative study of three model predictive current control methods with two vectors for three-phase DC/AC VSIs," *IET Electric Power Appl.*, vol. 11, no. 7, pp. 1284–1297, Aug. 2017.

[36] T. Jin, J. Guo, M. A. Mohamed, and M. Wang, "A novel model predictive control via optimized vector selection method for common-mode voltage reduction of three-phase inverters," *IEEE Access*, vol. 7, pp. 95351–95363, 2019.

[37] X. Shi, "Advanced control of three-phase full-bridge converter in microgrids," Ph.D. dissertation, Dept. Elect. Data Eng., Univ. Technol. Sydney, Ultimo, Australia, 2017.

JIANGUO ZHU (Senior Member, IEEE) received the B.E. degree from the Jiangsu Institute of Technology, China, in 1982, the M.E. degree from the Shanghai University of Technology, Shanghai, China, in 1987, and the Ph.D. degree from the University of Technology Sydney (UTS), Sydney, Australia, in 1995.

He is currently a Professor of electrical engineering and the Head of the School of Electrical and Information Engineering, The University of Sydney. His research interests include electromagnetics, magnetic properties of materials, electrical machines and drives, power electronics, and renewable energy systems.

LI LI (Member, IEEE) received the B.S. degree from the Huazhong University of Science and Technology, Wuhan, China, in 1996, the M.S. degree from Tsinghua University, Beijing, China, in 1999, and the Ph.D. degree from the University of California at Los Angeles, Los Angeles, CA, USA, in 2005.

From 2005 to 2007, he was a Research Associate with the University of New South Wales, Australian Defence Force Academy (UNSW ADFA), Canberra, ACT, Australia. From 2007 to 2011, he was a Researcher with National ICT Australia, Victoria Research Laboratory, Department of Electrical and Electronics Engineering, The University of Melbourne, Melbourne, VIC, Australia. He held several visiting positions at the Beijing Institute of Technology, Beijing, Tsinghua University, and UNSW ADFA. He joined the University of Technology Sydney, Ultimo, NSW, Australia, in 2011, where he is currently a Senior Lecturer. His current research interests are control theory and power system control.

DYLAN DAH-CHUAN LU (Senior Member, IEEE) received the Ph.D. degree in electronics and information engineering from The Hong Kong Polytechnic University, Hong Kong, in 2004. In 2003, he joined PowerELab Ltd., as a Senior Design Engineer, where he was responsible for industrial switching power supply projects. He was a full-time Faculty Member of The University of Sydney, from 2006 to 2016, where he currently holds an honorary position. Since July 2016, he has been an Associate Professor with the School of Electrical and Data Engineering, University of Technology Sydney, Australia. He has been heading the discipline of electrical power and energy systems, since December 2018. He has authored or coauthored more than 100 international journals and held two patents in power electronics. His current research interests include efficient and reliable power conversion for renewable sources, energy storage systems, and microgrids. He is currently serving as a Chair of the IEEE NSW Joint Chapter IAS/IES/PELS and an Associate Editor for the IEEE Transactions on Industrial Electronics.

XIAOLONG SHI (Student Member, IEEE) received the B.E. and M.E. degrees in electrical engineering from Beijing Jiaotong University, China, in 2011 and 2014, respectively, and the Ph.D. degree from the University of Technology Sydney (UTS), Sydney, NSW, Australia, in 2017.

Since 2013, he has been with the School of Data and Electrical Engineering, UTS. His research interests include design, optimization, advanced control algorithms of power converters and renewable energy systems, and advanced digital control with real-time implementation.

• • •